PCCP
Physical Chemistry Chemical Physics

Accepted Manuscript

This article can be cited before page numbers have been issued, to do this please use: E. Hosseini-Bab-Anari, A. M. Navarro-Suárez, K. Moth-Poulsen and P. Johansson, *Phys. Chem. Chem. Phys.*, 2019, DOI: 10.1039/C9CP03445E.

View Article Online
DOI: 10.1039/C9CP03445E

ARTICLE

Ionic liquid based battery electrolytes by lithium and sodium pseudo-delocalized pyridinium anion salts †

Received 00th January 20xx,
Accepted 00th January 20xx

DOI: 10.1039/x0xx00000x

Elham Hosseini-Bab-Anari,[a‡] Adriana M. Navarro-Suárez,[*b‡] Kasper Moth-Poulsen[a] and Patrik Johansson[*b,c]

The electrolyte salt plays an important role for the overall performance and safety of lithium- and sodium-ion batteries (LIBs and SIBs, respectively). Here, two new lithium and sodium pseudo-delocalized pyridinium anion based salts were used to prepare ionic liquid (IL) based electrolytes. The Li and Na salts of the 1-methylpyridinum 2,6-dicarboxylate anion (MM26py) were synthesized and dissolved in an IL matrix ($Pyr_{14}TFSI$) – hence creating mixed anion electrolytes. The obtained electrolytes are stable up to 150 and 200 °C and show ion conductivities of 2.8 and 3.2 $mS.cm^{-1}$ at room temperature, for the LIB and SIB electrolytes, respectively. A competitive effect between the MM26py and the TFSI anions to coordinate the alkali metal cations is observed. Finally, the electrochemical stability windows of 2.3 and 2.5 V, respectively, confirm that these electrolytes can be used practically in medium-voltage LIBs and SIBs.

Introduction

Safety and sustainability are key parameters of modern rechargeable batteries, where the electrolyte is a main aspect significantly impacting the battery cell safety, thermal stability, and abuse tolerance.[1,2] Designing novel battery electrolytes involves matching multiple performance criteria such as high ion conductivity, wide operating temperature range, and suitable electrochemical stability window.[3] There is a direct relationship between these criteria and the properties of the electrolyte that typically is composed of salt(s), solvent(s), and additives.

In order to achieve safer and also more sustainable batteries, some of us have previously designed fluorine-free anions based on the concept of pseudo-delocalization.[4,5] This entails salts based on anions with two negatively charged groups covalently attached to a central positively charged moiety. In our previous works aliphatic fluorine-free lithium and sodium salts were synthesized and characterized as prospective low voltage battery electrolyte components[6] and solvent-free electrolytes.[7] Ionic liquids (ILs) in general have low toxicity, high thermal stability, low vapour pressure and flammability – hence promising with respect to safety.[8] While many different ILs have been applied as lithium and sodium battery electrolyte matrices, especially by varying the anions of the ILs, they must be doped with alkali salts to be relevant for battery usage.[9–14] Furthermore, combining two different anions originating from a Li-/Na-salt and the IL matrix, *e.g.* using the popular anions bis(trifluoromethanesulfonyl)imide (TFSI) and bis(fluorosulfonyl)imide (FSI) in electrolytes, has resulted in enhanced ion conductivities[10] and battery performance[13] as compared to electrolytes with only one of these anions.[10,15,16] Herein, we combined the above observations by studying the effect of having both pseudo-delocalized and TFSI anions present in the electrolytes. Moreover, we here extend the family of pseudo-delocalized anions to aromatic systems for the first time, by preparing and characterizing lithium and sodium salts of the 1-methylpyridinum 2,6-dicarboxylate (MM26py) anion. These salts are dissolved in 1-butyl-1-methyl-pyrrolidinium TFSI ($Pyr_{14}TFSI$, also known as BmpyrTFSI, $BmpyrNTf_2$ or $Pyr_{14}NTf_2$) and we then study both basic physico-chemical properties such as local structure and thermal stability as well as battery relevant properties such as ion conductivities and electrochemical stability windows, to evaluate their possible use as battery electrolytes.

Experimental

Materials and methods

All chemicals were used without any further purification. Dimethyl 2,6-pyridinedicarboxylate, diethyl ether, ethyl acetate, anhydrous dichloromethane (DCM, ≥99.8%), sodium hydroxide pellet (NaOH, ≥97%), methyl trifluoromethanesulfonate (MeOTF, ≥98%), lithium hydroxide powder (LiOH, ≥98%), deuterium oxide, ethanol (C_2H_5OH, ≥98%) ethylene carbonate (EC, anhydrous, 99%), and dimethyl carbonate (DMC, anhydrous, ≥99%) were all purchased from Sigma-Aldrich. Lithium bis(trifluoromethanesulfonyl)imide

[a] Department of Chemistry and Chemical engineering, Chalmers University of Technology, SE-412 96 Gothenburg, Sweden
[b] Department of Physics, Chalmers University of Technology, SE-412 96 Gothenburg, Sweden
[c] ALISTORE – European Research Institute, CNRS FR 3104, Hub de l'Energie, 15 Rue Baudelocque, 80039 Amiens, France
* Corresponding authors: asuarez@chalmers.se, patrik.johansson@chalmers.se
†Electronic Supplementary Information (ESI) available. See DOI: 10.1039/x0xx00000x
‡ These authors have contributed equally to this paper.

(LiTFSI, 99.9%), sodium bis(trifluoromethanesulfonyl)imide (NaTFSI, 99.5%) and 1-butyl-1-methylpyrrolidinium bis(trifluoromethanesulfonyl)imide (Pyr_{14}TFSI, 99.9%) were purchased from Solvionic.

Synthesis procedure

2,6-Dimethoxycarbonyl-1-methylpyridinium trifluoromethanesulfonate. According to a previously reported method,[17,18] dimethyl 2,6-pyridinedicarboxylate (3.73 g, 19.1 mmol) was here dissolved in 20 mL of anhydrous dichloromethane and methylated under reflux at 40 °C by adding a solution of methyl trifluoromethanesulfonate (3 mL, 26.5 mmol) in 30 mL of anhydrous dichloromethane over 3 weeks (Scheme 1). The reaction mixture was cooled to room temperature, 200 mL of diethyl ether were added and then it was further cooled to ~5 °C. The crude needle-like product was left to precipitate during a 24 h period. Recrystallization of the crude product from ethyl acetate and drying in vacuum oven at 50 °C for 24 h yielded pure colourless crystalline 2,6-dimethoxycarbonyl-1-methylpyridinium trifluoromethanesulfonate (6.58 g, 18.3 mmol) corresponding to 96 % yield based on dimethyl 2,6-pyridinedicarboxylate.

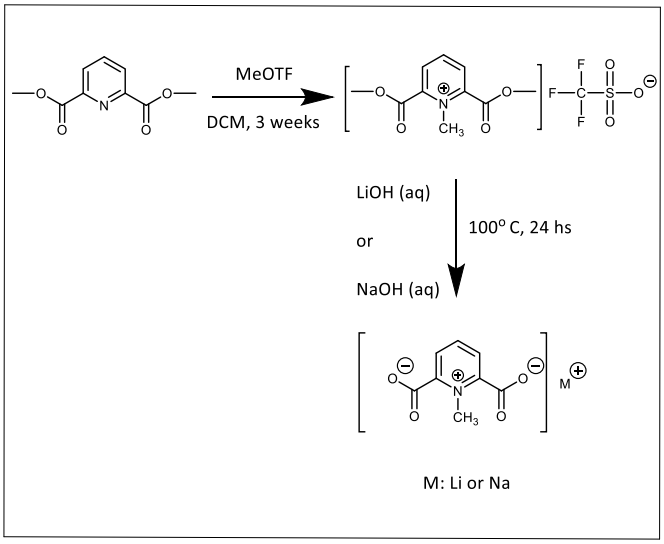

Scheme 1. Synthesis path for MM26py and its Li and Na salts.

Lithium and sodium 1-methylpyridinium 2,6-dicarboxylate (LiMM26py and NaMM26py). In the second step hydrolysis of 2,6-dimethoxycarbonyl-1-methylpyridinium trifluoromethanesulfonate (3 g, 8.34 mmol) with 2 equimolar of the respective base (sodium hydroxide (0.667 g, 16.68 mmol) or lithium hydroxide (3 g, 16.68 mmol)) was performed in 20 mL of water at 100 °C for 24 h. After cooling the reaction mixture to room temperature, water was removed using high vacuum rotavapor. The crude salts were further purified by recrystallization from methanol, followed by drying in a vacuum oven at 50 °C, yielding LiMM26py (1.34 g, 7.16 mmol, 86%) and NaMM26Py (1.4 g, 6.89 mmol, 83%) as analytically pure colourless crystalline products.

Nuclear Magnetic Resonance and Elemental Analysis. ^{1}H and ^{13}C NMR spectroscopy were carried out using an automated Bruker 400 MHz spectrometer at 298 K. Chemical shifts are reported in parts per million (ppm) referring to the internal residual proton signal (D_2O: 4.64 ppm). All the NMR spectra are available in the ESI (Figs. S1-S4). The elemental analysis data were collected as a service provided by Mikrolab Kolbe AG, Germany.

2,6-Dimethoxycarbonyl-1-methylpyridinium trifluoromethanesulfonate: ^{1}H-NMR (400 MHZ, D_2O): 3.99 (s, 6H, 2xOCH_3); 4.43 (s, 3H, NCH_3); 8.46 (d, 2H, 2xCH); 8.7 (t, 1H, CH). ^{13}C-NMR (100 MHz, D_2O): 45.92 (NCH_3); 55.01 (2xOCH_3); 131.47 (2xCH and CF); 146.2 (2xCC); 147.8 (CH) 160.6 (2xCO_2).

LiMM26py: ^{1}H-NMR (400 MH_z, D_2O) δ = 4.14 (s, 3H, NCH_3); 7.77 (d, 2H, 2xCH); 8.37 (t, 1H, CH) ppm. ^{13}C-NMR (100 MH_z, D_2O) δ: 43.3 (NCH_3); 124.3 (2xCH); 146.8 (CH); 152.3 (2xCC); 165.9 (CO_2) ppm. Elem. Anal.: Calc. ($LiC_8H_6NO_4$. 0.6 H_2O): C, 48.56; H, 3.67; N, 7.08; Li, 3.51. Found: C, 48.44; H, 3.99; N, 7.18; Li: 3.53. LC-MS: m/z=182 (M^-_{anions}+2), 180 (M^-_{anions}).

NaMM26py: ^{1}H-NMR (400 MH_z, D_2O) δ = 4.14 (s, 3H, NCH_3); 7.77 (d, 2H, 2xCH); 8.37 (t, 1H, CH) ppm. ^{13}C-NMR (100 MH_z, D_2O) δ: 43.3 (NCH_3); 124.3 (2xCH); 146.8 (CH); 152.3 (2xCC); 165.9 (CO_2) ppm. Elem. Anal.: Calc. ($NaC_8H_6NO_4$. 0.45 H_2O): C, 45.49; H, 3.29; N, 6.63; Na, 10.88. Found: C, 45.55; H, 3.55; N, 6.97; Na: 10.87. LC-MS: m/z=182 (M^-_{anions}+2), 180 (M^-_{anions}).

Solubility tests

Solubility tests were performed by adding Pyr_{14}TFSI, EC:DMC 1:1, and water, to 100 mg of LiMM26py and NaMM26py salts and subsequently mixing with a magnetic stirrer. The solubility was evaluated by visual inspection.

Electrolyte preparation

LiMM26py and NaMM26py were dried under vacuum in a Büchi oven at 60 °C for 3 days. The water content was determined to be < 5 ppm by titration using a Metrohm 381 Karl-Fischer Coulometer. $[LiMM26py]_{0.1}[Pyr_{14}TFSI]_{0.9}$ and $[NaMM26py]_{0.1}[Pyr_{14}TFSI]_{0.9}$ electrolytes were prepared by direct mixing of the appropriate amounts of salt and IL. $[Li]_{0.1}[Pyr_{14}]_{0.9}$TFSI and $[Na]_{0.1}[Pyr_{14}]_{0.9}$TFSI were also prepared as references. All materials were stored and handled in an argon filled glove box (H_2O < 1 ppm, O_2 < 1 ppm).

Thermal analysis

The thermal stability was studied by thermogravimetric analysis (TGA) for samples of ~20 mg using a Netzsch TG 209 F1 instrument with a resolution of 0.1 µg under N_2 gas atmosphere with a flow of 20 mL.min^{-1} and a heating rate of 5 °C.min^{-1}. The extrapolated onset temperatures, *i.e.* the intersection point of the extrapolated baseline and the inflectional tangent at the beginning of the mass losses, are reported.

Journal Name ARTICLE

View Article Online
DOI: 10.1039/C9CP03445E

Melting points and phase transformation temperatures were obtained through differential scanning calorimetry (DSC, TA Instruments Q1000) for samples of ~10 mg using sealed aluminium pans. A heating rate of 10 °C.min^{-1} was used. The extrapolated onset temperatures, *i.e.* the intersection point of the extrapolated baseline and the inflectional tangent at the beginning of the transitions, are reported.

Raman spectroscopy

To study the local coordination we used Fourier transform Raman spectroscopy at room temperature using a Bruker MultiRAM spectrometer, with a nitrogen-cooled germanium detector and a resolution of 2 cm^{-1}. A Nd-YAG (1064 nm) laser was used at an operating power of 200 mW and the Raman spectra were derived from 1000-2000 scans. For a detailed analysis of the region 725–765 cm^{-1}, sensitive to TFSI anion coordination, the spectra were fitted using pseudo-Voigt functions (Gaussian:Lorentzian = 60:40), following the procedure of Lassègues *et al.*[19]

Solvation numbers (SN) for the metal cations were calculated from the deconvoluted Raman spectra in accordance with the procedure of Pitawala *et al.*;[20] dividing the area of the band corresponding to coordinated TFSI (A_C) by the total band area ($A_C + A_F$ (="free" TFSI)) and the molar fraction of metal-salt (0.1).

$$SN = \frac{A_C/(A_C+A_F)}{0.1} \qquad \text{eq. 1}$$

Broadband dielectric spectroscopy

A Novocontrol broadband dielectric spectrometer equipped with an Alpha-S high-resolution dielectric analyser was used to obtain the ion conductivities. A cell with blocking stainless steel electrodes, an inner diameter of 4 mm and a thickness of 1 mm, both defined by a PTFE spacer was used. The cell was filled with sample inside the argon glove box for inert transfer to the instrument. The measurements were performed on both the heating and the cooling ramp. Starting at 0 °C, the sample was heated to 100 °C and then cooled to 0 °C in 10 °C steps, using a 15 min equilibration time before measurement at each temperature, from 10^{-2} to 10^{7} Hz and a 10 mV RMS AC perturbation. The ion conductivities are read from the high frequency plateau, *e.g.* 316 kHz (Fig. S5).

The relationship between temperature (T) and ion conductivity (σ) was fitted using the Vogel-Fulcher-Tammann (VFT) equation,

$$\sigma = \sigma_0 \times e^{-\frac{B}{T-T_0}} \qquad \text{eq. 2}$$

where σ_0 is the prefactor often related to the charge carrier concentration, while *B* is an empirical parameter characteristic of the material and related to the apparent activation energy at a given temperature. T_0, also known as the Vogel temperature, is the temperature at which the configurational entropy becomes zero.[21] All fitting was performed by using a Levenberg–Marquardt algorithm in the Origin Lab® software.

Angell's strength parameter D_σ is often used to classify the fragility of liquids and was calculated using eq. 3.

$$D_\sigma = \frac{B_\sigma}{T_0} \qquad \text{eq. 3}$$

Electrochemical stability window (ESW)

The ESW was obtained by cyclic voltammetry (CV) on coin cells at room temperature, using nickel foil as working electrode (WE) and lithium/sodium foil as a counter (CE) and reference electrode (RE). The 2032 coin cells were assembled using 12 mm electrodes, 14 mm glass microfibre filters (Whatman, GF/A, 0.26 mm thick) separators, and 60 µl electrolyte. All cells were assembled in an Ar-filled glovebox (H_2O < 1 ppm, O_2 < 1 ppm). The voltammograms were recorded using a Biologic SA MPG instrument using the EC-Lab software between -1 and 6 *vs*. Li^+/Li and Na^+/Na, respectively, and a scan rate of 1 mV.s^{-1}.

Results and discussion

First, we describe the synthesis methods for the novel lithium and sodium pseudo-delocalized pyridinium anion salts and then we compare the physico-chemical properties of four Pyr_{14}TFSI-based electrolytes containing either one anion, *i.e.* TFSI as reference (Fig. 1a), or two anions, *i.e.* TFSI and MM26py (Fig. 1b). We focus on revealing the influence of MM26py on thermal stability, local structure of TFSI, ion conductivity and electrochemical stability window.

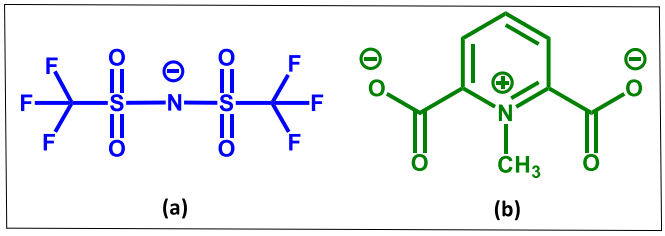

Fig 1. Chemical structures of (a) bis(trifluoromethanesulfonyl)imide (TFSI) and (b) 1-methylpyridinum 2,6-dicarboxylate (MM26py).

Synthesis of LiMM26py and NaMM26py

The synthesis of LiMM26py and NaMM26py were carried out via a two step-procedure. In the first step, pyridine 2,6-dicarboxylate dimethylester was N-alkylated using methyl trifluoromethanesulfonate (MeOTF) as an alkylation agent. Due to both steric and electronic effects, the reactivity of the pyridine is somewhat low.[18] Inspired by Wang *et al.*[17] we used the MeOTF alkylation agent and by reducing the amount of MeOTF to ~1.3 molar equivalent and increasing the reaction time to 3 weeks, the reaction yield increased from previously reported 53%[17] to 96%. In the second step, hydrolysis of the ester was carried out in basic solution, not only due to the need of metal cation (Li, Na) as a counter-ion, but also because of the irreversibility of the ester hydrolysis reaction under basic conditions. Furthermore, the ester hydrolysis under basic conditions resulted in much higher yields (LiMM26py: 86% and NaMM26py: 83%) as compared to under acidic conditions (12%

yield).[17] Combined these optimized synthesis procedures furnish the target salts in excellent yield with high analytical purity.

Solubility tests

High solubility in the matrix, being it water, organic solvent, or an IL, is a prerequisite when selecting an electrolyte salt. The solubility of LiMM26py and NaMM26py at room temperature in various solvents (Table 1) show that while both salts have excellent solubilities in both water and $Pyr_{14}TFSI$ as compared to our previously synthesised pseudo-delocalized anion salts,[6] the solubilities are low in the standard LIB electrolyte EC:DMC 1:1 solvent mixture (Table 1). The value reported corresponds to the minimum concentration investigated. We speculate that the variation in solubility is due to strong interactions between the two CO_2^- groups and Li^+ and Na^+ ions, which only highly polar solvents with high dielectric constants or protic solvents, *e.g.* $Pyr_{14}TFSI$ or water, can disrupt.

Table 1. Solubility of LiMM26py and NaMM26py

Salt	Solubility [m]		
	Water	EC:DMC 1:1	$Pyr_{14}TFSI$
LiMM26py	<9.0	<2.6E-4	<0.5
NaMM26py	<8.2	<2.4E-4	<0.5

Thermal analysis

Thermal stability is an important factor for LIB and SIB electrolytes for both safety, operation conditions and life-length.[24] The thermogravimetric analysis (TGA) for each of the $Pyr_{14}TFSI$-based electrolytes, the neat salts and the IL show the reference $[Li]_{0.1}[Pyr_{14}]_{0.9}TFSI$ (Fig. 2a) and $[Na]_{0.1}[Pyr_{14}]_{0.9}TFSI$ (Fig. 2b) electrolytes to be significantly more robust than the MM26py-based electrolytes (Fig. 2c, d). This is due to the higher thermal stabilities of the LiTFSI and NaTFSI salts as compared to the LiMM26py and NaMM26py salts. The LiMM26py (Fig. 2c) and NaMM26py (Fig. 2d) salts showed initial weight losses at ~150 and 200 °C, respectively, which corresponds mainly to decarboxylation processes (Fig. S6) as has also been observed for other pyridine compounds.[25] At 550 °C, the residuals of LiMM26py and NaMM26py, respectively, are 38 and 50 %. The $[LiMM26py]_{0.1}[Pyr_{14}TFSI]_{0.9}$, and $[NaMM26py]_{0.1}[Pyr_{14}TFSI]_{0.9}$ electrolytes lost mass at 150 and 200 °C, respectively, hence at the same temperatures as the salts decompose.

We performed DSC measurements (Fig. 3) on the various salts and electrolytes in order to determine any phase transitions and the practical operation temperature ranges. $Pyr_{14}TFSI$ showed a sharp crystallization peak at -54 °C and a melting peak at -19 °C, both in good agreement with the literature.[26] When LiTFSI (Fig. 3a) and NaTFSI (Fig. 3b) salts are added, the crystallization and melting peak areas decrease significantly, and for $[Na]_{0.1}[Pyr_{14}]_{0.9}TFSI$ (Fig. 3b) they completely disappear, which agrees with previous reports.[14,27] The extra endothermic peak in the $[Li]_{0.1}[Pyr_{14}]_{0.9}TFSI$ electrolyte (Fig. 3a) points towards the existence of more than one crystalline phase.[26]

The DSC traces for the pure salts (Figs. 3c-d) do not show any phase transitions in the temperature range studied (-90 - 150 °C). When LiMM26py is added to the IL (Fig. 3c), the crystallization peak of the IL maintains its position and area, but the melting peak moves to -5 °C (Δ = 14 °C) and the area of the peak increases. In contrast, the addition of NaMM26py (Fig. 3d) decreases the IL crystallization temperature to -57 °C (Δ = -3 °C)

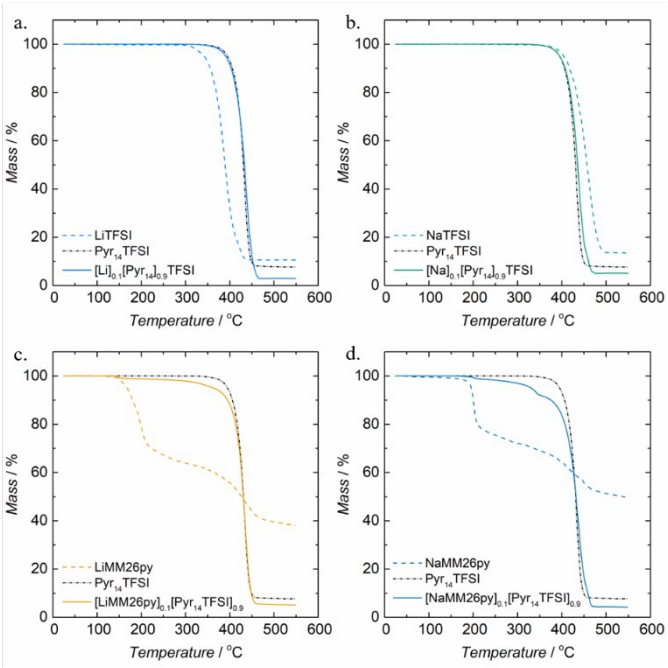

Fig 2. TGA heating thermograms of: (a) $[Li]_{0.1}[Pyr_{14}]_{0.9}TFSI$, (b) $[Na]_{0.1}[Pyr_{14}]_{0.9}TFSI$, (c) $[LiMM26py]_{0.1}[Pyr_{14}TFSI]_{0.9}$, and (d) $[NaMM26py]_{0.1}[Pyr_{14}TFSI]_{0.9}$. The pure salts and $Pyr_{14}TFSI$ are included for comparison.

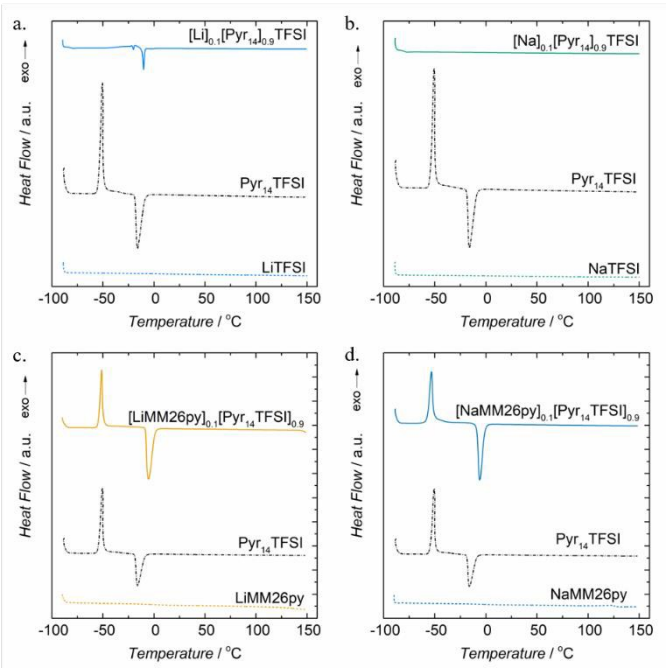

Fig 3. DSC heating curves (5 °C.min^{-1}) of (a) $[Li]_{0.1}[Pyr_{14}]_{0.9}TFSI$, (b) $[Na]_{0.1}[Pyr_{14}]_{0.9}TFSI$, (c) $[LiMM26py]_{0.1}[Pyr_{14}TFSI]_{0.9}$, and (d) $[NaMM26py]_{0.1}[Pyr_{14}TFSI]_{0.9}$. Their respective salts and $Pyr_{14}TFSI$ are included for comparison.

and increases the melting temperature to -8 °C (Δ = 11 °C). These effects might be due to an increased ionic order in the solid phases preceding the melting.[26]

Raman spectroscopy

The local coordination of the TFSI anion by alkali cations has been extensively studied by Raman spectroscopy. Two stable conformers of TFSI, which are sensitive to both conformation and coordination changes,[19,20,28,29] co-exist in electrolytes at RT and spectroscopically give rise to two closely spaced ''free'' anion bands at 738 and 741 cm^{-1} – observed as a single envelope at ~742 cm^{-1}.[28,29] Here the Raman spectrum of $Pyr_{14}TFSI$ showed a band centred at 741 cm^{-1} (Figs. 4a and b) formed by the two overlapping bands corresponding to the ''free'' TFSI anion. Addition of LiTFSI led to a new band, at 748 cm^{-1}, due to the formation of $[Li(TFSI)_n]^{1-n}$ complexes.[19] When NaTFSI was added, a band corresponding to $[Na(TFSI)_n]^{1-n}$ complexes appeared at 746 cm^{-1}, indicating a weaker Na^+-TFSI interaction due to the smaller charge/radius ratio of the sodium cation as compared to the lithium cation.[30] The average solvation number (SN) of Li^+ and Na^+ by TFSI was 1.9 and 2.6, respectively, in agreement with previous studies.[30,31]

Addition of LiMM26py and NaMM26py to $Pyr_{14}TFSI$ led to the bands corresponding to the $[Li(TFSI)_n]^{1-n}$ and $[Na(TFSI)_n]^{1-n}$ complexes at 747 and 744 cm^{-1}, respectively, to appear. This indicates that by adding a salt with a different anion than in the IL, the M^+-TFSI interactions become less pronounced due to a competitive coordination by the MM26py anion, where Na^+ seems to preferentially coordinate MM26py anion relatively to Li^+, as also confirmed by the Vogel temperatures (T_0, see Table 2) calculated from the conductivity results. Moreover, between Li and Na-TFSI ion-pairs the interaction energy difference is

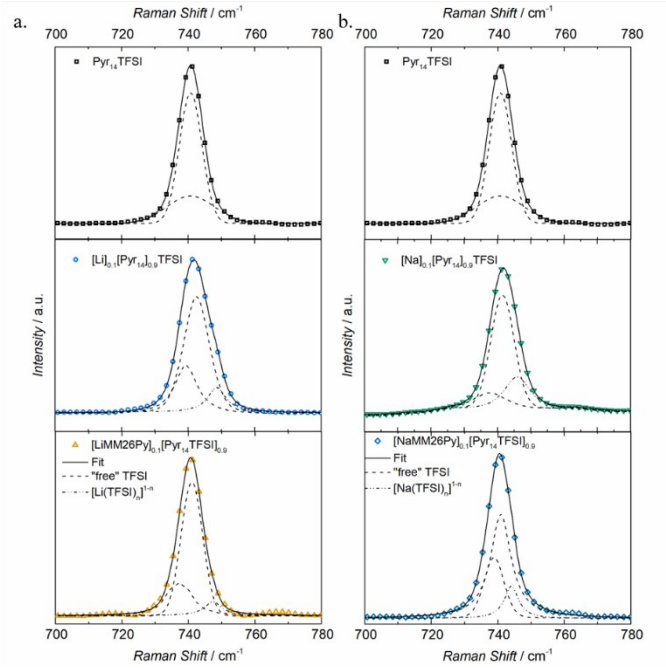

Fig 4. Deconvoluted Raman spectra of: (a) the lithium and (b) the sodium based electrolytes prepared. $Pyr_{14}TFSI$ is included for comparison.

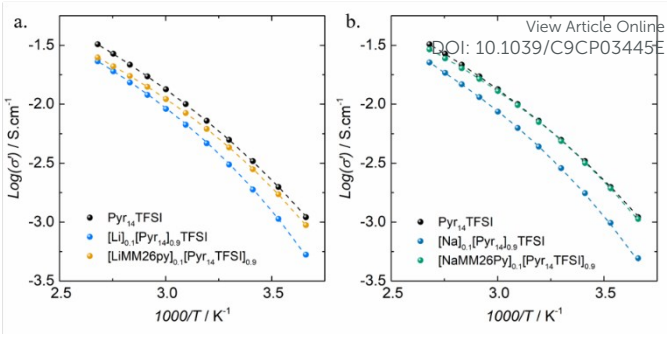

Fig. 5. Arrhenius plots of the (a) lithium, and (b) sodium based electrolytes. $Pyr_{14}TFSI$ is included for comparison.

~100 kJ.mol^{-1}, smaller for Na^+, while at the same DFT level (B3LYP) the difference for Li^+ *vs.* TFSI and MM26py is only 24 kJ.mol^{-1}, smaller for MM26py.[32] As a result, the M^+ anion SN for $[LiMM26py]_{0.1}[Pyr_{14}TFSI]_{0.9}$, and $[NaMM26py]_{0.1}[Pyr_{14}TFSI]_{0.9}$ were 0.9 and 1.1, respectively. The presence of more "free" TFSI anions in these electrolytes might explain the similarities in the DSC curves of $[LiMM26py]_{0.1}[Pyr_{14}TFSI]_{0.9}$, $[NaMM26py]_{0.1}[Pyr_{14}TFSI]_{0.9}$, and $Pyr_{14}TFSI$.

Ion conductivities

The electrolyte ion conductivity is a crucial factor for cell performance, and in general, IL based electrolytes present lower ion conductivities than the neat IL, given that the salt alkali cations create large complexes with the IL anions.[26] Here the ion conductivities of both $[LiMM26py]_{0.1}[Pyr_{14}TFSI]_{0.9}$ and $[NaMM26py]_{0.1}[Pyr_{14}TFSI]_{0.9}$ were higher than the ion conductivities of $[Li]_{0.1}[Pyr_{14}]_{0.9}TFSI$ and $[Na]_{0.1}[Pyr]_{0.9}TFSI$ in the whole temperature range studied (Fig. 5). This is due to the higher number of "free" TFSI anions observed by the Raman spectroscopy analysis.

The ion conductivities were fitted upsing the VFT equation and from the fitting parameters (Table 2) it is clear that the number of charge carriers, related to σ_0, decrease when adding the lithium and sodium salts to the IL – hence yet a sign of interactions between the alkali cations and the electrolyte anions. As observed by the Raman spectroscopy analysis, adding LiMM26py and NaMM26py increases the relative amount of "free" TFSI anions, explaining why σ_0 for the electrolytes based on these salts were higher than for those with only a single type of anion *i.e.* $[Li]_{0.1}[Pyr_{14}]_{0.9}TFSI$ and $[Na]_{0.1}[Pyr_{14}]_{0.9}TFSI$. Though the carrier ion number decreased in comparison with $Pyr_{14}TFSI$, the apparent activation energy (B_σ) also decreased, allowing for a high ion conductivity of the electrolytes $[LiMM26py]_{0.1}[Pyr_{14}TFSI]_{0.9}$ and $[NaMM26py]_{0.1}[Pyr_{14}TFSI]_{0.9}$.

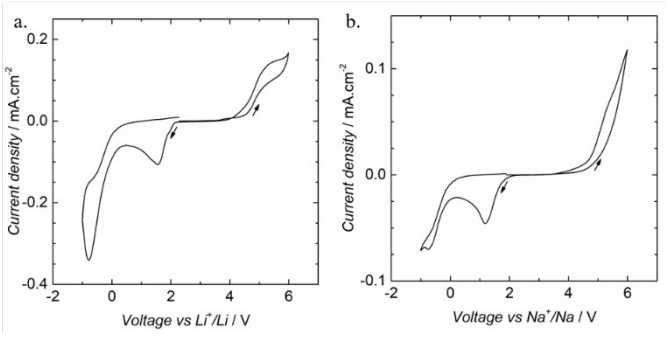

Fig. 6. CVs between -1 and 6 V for: (a) $[LiMM26py]_{0.1}[Pyr_{14}TFSI]_{0.9}$ and (b) $[NaMM26py]_{0.1}[Pyr_{14}TFSI]_{0.9}$.

Table 2. VFT fitting parameters for pure $Pyr_{14}TFSI$ and the lithium and sodium based electrolytes.

	σ_0 (S.cm^{-1})	B_σ (K)	T_0 (K)	D_σ
$Pyr_{14}TFSI$	2.69	832.1	158.0	5.3
$[Li]_{0.1}[Pyr_{14}]_{0.9}TFSI$	0.32	656.1	182.6	3.6
$[Na]_{0.1}[Pyr_{14}]_{0.9}TFSI$	0.45	778.4	172.0	4.5
$[LiMM26py]_{0.1}[Pyr_{14}TFSI]_{0.9}$	0.48	630.5	175.7	3.6
$[NaMM26py]_{0.1}[Pyr_{14}TFSI]_{0.9}$	1.20	622.3	177.7	3.5

An increasing Vogel temperature, T_0, upon salt doping has previously been related to the formation of alkali cation:anion complexes with significantly reduced mobilities.[31,33] Here the $[Li]_{0.1}[Pyr_{14}]_{0.9}TFSI$ electrolyte exhibited the highest Vogel temperature, which might be associated with the extra crystalline phase observed by DSC and the strong interactions between Li^+ and TFSI. In contrast, $[Na]_{0.1}[Pyr_{14}]_{0.9}TFSI$, due to the weaker ion-ion interactions between Na^+ and TFSI than for Li^+ *vs.* TFSI, present a lower T_0 even if still higher than for the pure $Pyr_{14}TFSI$ IL. Angell's strength parameter is $3.5 < D_\sigma < 4.5$ for the electrolytes. Pure $Pyr_{14}TFSI$ has already been investigated by Harris *et al.*[34] and a comparable, but higher D_σ (5.4) was obtained. All our systems can be classified as fragile ($D_\sigma < 30$), due to cations and anions being coupled, in accordance with the IL electrolyte literature.[14,35]

Electrochemical stability window (ESW)

The CV evaluation of the electrochemical stability windows of the $[LiMM26py]_{0.1}[Pyr_{14}TFSI]_{0.9}$ and $[NaMM26py]_{0.1}[Pyr_{14}TFSI]_{0.9}$ electrolytes show the former to exhibit a reduction peak at 1.56 V *vs*. Li^+/Li and the latter a similar feature at 1.19 V *vs*. Na^+/Na, with onsets at ~2 V. Based on the metals' standard electrode potentials, -3.05 V for lithium and -2.71 V for sodium, these features are most likely caused by the same reaction. In the literature,[36] $[Li]_{0.1}[Pyr_{14}]_{0.9}TFSI$ and $Pyr_{14}TFSI$ have shown stability down to -0.1 V *vs.* Li^+/Li, showing that nor Pyr_{14} nor TFSI are responsible for these peaks. Therefore, the above features are ascribed to the reduction of the MM26py anion. Moreover, it is not due to any minor impurity as the features increase in each of the multiple scans and this also indicates that no passivation layer is formed. In terms of anodic stability, $[LiMM26py]_{0.1}[Pyr_{14}TFSI]_{0.9}$ and $[NaMM26py]_{0.1}[Pyr_{14}TFSI]_{0.9}$ start to decompose at 4.3 V *vs*. Li^+/Li and 4.5 V *vs*. Na^+/Na, respectively. Hence the ESWs allow these electrolytes to be used in LIBs and SIBs with operating voltages $2 < V < 4.3$ *vs*. Li^+/Li and $2 < V < 4.5$ *vs*. Na^+/Na.

Conclusions

Synthesis of new Li/Na-salts based on pseudo-delocalized pyridinium anions can be accomplished from low cost and readily available starting materials. Since no column chromatography for purification is needed, the scale-up of this synthesis method to kg scale can be straight-forward. The high solubility of LiMM26py and NaMM26py in ILs allow them to be used in IL based electrolytes. Adding LiMM26py and NaMM26py to $Pyr_{14}TFSI$ reduces the thermal stability, which we speculate can be improved upon by replacing the CO_2^- moieties by SO_3^-. The Raman analysis of the electrolytes infers a MM26py/TFSI mixed solvation of the cations and also various charge carriers to be possible. The higher conductivities of IL based electrolytes containing pseudo-delocalized anions reveal a positive effect in a wide temperature range. Overall, low synthesis cost, high ion conductivity with reasonable thermal and electrochemical stability, demonstrate the potential for application of these non-fluorinated salts in LIB and SIB electrolytes. While the concept cannot at this early stage compete in stability or cycling efficiency measures we do believe understanding these salts better is a stepping stone towards performant totally non-fluorinated electrolytes for lithium- and sodium-ion batteries and such would also be better at the battery recycling stage due to being fluorine-free.

Conflicts of interest

There are no conflicts to declare.

Acknowledgements

The financial support by the Swedish Energy Agency ("Batterifonden" grants #37671-1 and #42762-1) is gratefully acknowledged. The authors are also grateful to Chalmers Battery Initiative and to several of Chalmers Areas of Advance; Energy, Materials Science, and Transport for continuous support.

Notes

‡ Electronic supplementary information (ESI) available:

References

1 K. Xu, *Chem. Rev.*, 2014, **114**, 11503–11618.
2 Z. Yang, J. Zhang, M. C. W. Kintner-Meyer, X. Lu, D. Choi, J. P. Lemmon and J. Liu, *Chem. Rev.*, 2011, **111**, 3577–3613.
3 D. Aurbach, Y. Talyosef, B. Markovsky, E. Markevich, E. Zinigrad, L. Asraf, J. S. Gnanaraj and H. J. Kim, *Electrochim. Acta*, 2004, **50**, 247–254.

4 US 2014/0272601 A1, 2014, 1–7.

5 E. Jónsson, M. Armand and P. Johansson, *Phys. Chem. Chem. Phys.*, 2012, **14**, 6021–6025.

6 E. Hosseini-Bab-Anari, A. Boschin, T. Mandai, H. Masu, K. Moth-Poulsen and P. Johansson, *RSC Adv.*, 2016, **6**, 85194–85201.

7 J. Forero-Saboya, E. Hosseini-Bab-Anari, M. E. Abdelhamid, K. Moth-Poulsen and P. Johansson, *Chem. Commun.*, 2019, **55**, 632–635.

8 E. Quartarone and P. Mustarelli, *Chem. Soc. Rev.*, 2011, **40**, 2525–2540.

9 M. Ishikawa, T. Sugimoto, M. Kikuta, E. Ishiko and M. Kono, *J. Power Sources*, 2006, **162**, 658–662.

10 M. Nádherná, J. Reiter, J. Moškon and R. Dominko, *J. Power Sources*, 2011, **196**, 7700–7706.

11 M. Yamagata, Y. Matsui, T. Sugimoto, M. Kikuta, T. Higashizaki, M. Kono and M. Ishikawa, *J. Power Sources*, 2013, **227**, 60–64.

12 Y. Matsui, M. Yamagata, S. Murakami, Y. Saito, T. Higashizaki, E. Ishiko, M. Kono and M. Ishikawa, *J. Power Sources*, 2015, **279**, 766–773.

13 A. Lahiri, T. J. S. Schubert, B. Iliev and F. Endres, *Phys. Chem. Chem. Phys.*, 2015, **17**, 11161–11164.

14 M. Kerner, N. Plylahan, J. Scheers and P. Johansson, *Phys. Chem. Chem. Phys.*, 2015, **17**, 19569–19581.

15 F. Mueller, N. Loeffler, G. T. Kim, T. Diemant, R. J. Behm and S. Passerini, *ChemSusChem*, 2016, **9**, 1290–1298.

16 S. Sayah, F. Ghamouss, F. Tran-Van, J. Santos-Peña and D. Lemordant, *Electrochim. Acta*, 2017, **243**, 197–206.

17 X. Bin Wang, J. E. Dacres, X. Yang, K. M. Broadus, L. Lis, L. S. Wang and S. R. Kass, *J. Am. Chem. Soc.*, 2003, **125**, 296–304.

18 A. R. Katritzky and F. Soti, *J. Chem. Soc. Perkin Trans. I*, 1974, 1427–1432.

19 J. C. Lassègues, J. Grondin, C. Aupetit and P. Johansson, *J. Phys. Chem. A*, 2009, **113**, 305–314.

20 A. Martinelli, J. Pitawala, A. Matic, P. Johansson and P. Jacobsson, *J. Non. Cryst. Solids*, 2014, **407**, 318–323.

21 K. M. Diederichsen, H. G. Buss and B. D. McCloskey, *Macromolecules*, 2017, **50**, 3831–3840.

22 C. A. Angell, R. D. Bressel, J. L. Green, H. Kanno, M. Oguni and E. J. Sare, *J. Food Eng.*, 1994, **22**, 115–142.

23 C. A. Angell, 2014, **267**, 1924–1935.

24 H. Che, S. Chen, Y. Xie, H. Wang, K. Amine, X. Z. Liao and Z. F. Ma, *Energy Environ. Sci.*, 2017, **10**, 1075–1101.

25 S. Mlowe, D. J. Lewis, M. Azad Malik, J. Raftery, E. B. Mubofu, P. O'Brien and N. Revaprasadu, *New J. Chem.*, 2014, **38**, 6073–6080.

26 A. Martinelli, A. Matic, P. Jacobsson, L. Börjesson, A. Fernicola and B. Scrosati, *J. Phys. Chem. B*, 2009, **113**, 11247–11251.

27 S. A. Mohd Noor, P. C. Howlett, D. R. Macfarlane and M. Forsyth, *Electrochim. Acta*, 2013, **114**, 766–771.

28 M. Herstedt, M. Smirnov, P. Johansson, M. Chami, J. Grondin, L. Servant and J. C. Lassègues, *J. Raman Spectrosc.*, 2005, **36**, 762–770.

29 S. Duluard, J. Grondin, J.-L. Bruneel, I. Pianet, A. Grélard, G. Campet, M.-H. Delville and J.-C. Lassègues, *J. Raman Spectrosc.*, 2008, **39**, 627–632.

30 D. Monti, E. Jónsson, M. R. Palacín and P. Johansson, *J. Power Sources*, 2014, **245**, 630–636.

31 J. Pitawala, J. K. Kim, P. Jacobsson, V. Koch, F. Croce and A. Matic, *Faraday Discuss.*, 2012, **154**, 71–80.

32 E. Jónsson and P. Johansson, *Phys. Chem. Chem. Phys.*, 2012, **14**, 10774.

33 M. J. Monteiro, F. F. C. Bazito, L. J. A. Siqueira, M. C. C. Ribeiro and R. M. Torresi, *J. Phys. Chem. B*, 2008, **112**, 2102–2109.

34 K. R. Harris, L. A. Woolf, M. Kanakubo and T. Rüther, *J. Chem. Eng. Data*, 2011, **56**, 4672–4685.

35 C. Austen Angell, Y. Ansari and Z. Zhao, *Faraday Discuss.*, 2012, **154**, 9–27.

36 G. B. Appetecchi, M. Montanino and S. Passerini, in *Ionic Liquids: Science and Applications*, eds. A. E. Visser, N. J. Bridges and R. D. Rogers, 2012, vol. 1117, pp. 67–128.

DOI: 10.1039/C9CP03445E